# A HOUGH TRANSFORM GLOBAL PROBABILISTIC APPROACH TO MULTIPLE SUBJECT DIFFUSION MRI TRACTOGRAPHY

By

**Iman Aganj, Christophe Lenglet**

**Neda Jahanshad, Essa Yacoub**

**Noam Harel, Paul M. Thompson**

and

**Guillermo Sapiro**

**IMA Preprint Series # 2305**

( April 2010 )

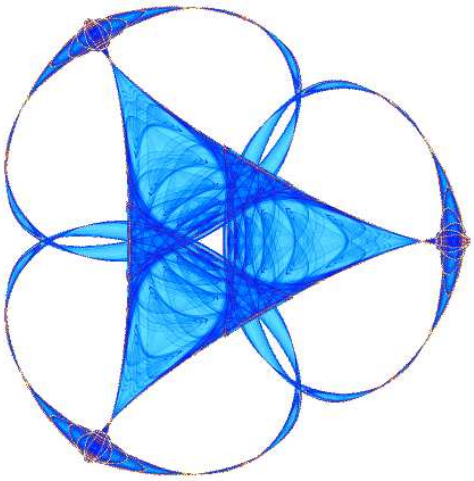

INSTITUTE FOR MATHEMATICS AND ITS APPLICATIONS

UNIVERSITY OF MINNESOTA

400 Lind Hall
207 Church Street S.E.
Minneapolis, Minnesota 55455–0436

Phone: 612-624-6066 Fax: 612-626-7370
URL: http://www.ima.umn.edu

# A Hough Transform Global Probabilistic Approach to Multiple-Subject Diffusion MRI Tractography

Iman Aganj,[a] Christophe Lenglet,[a,b] Neda Jahanshad,[c] Essa Yacoub,[b] Noam Harel,[b] Paul M. Thompson,[c] and Guillermo Sapiro[a]

[a] Department of Electrical and Computer Engineering, University of Minnesota, Minneapolis, 200 Union St. SE, MN 55455, USA

[b] Center for Magnetic Resonance Research, University of Minnesota, 2021 Sixth Street SE, Minneapolis, MN 55455, USA

[c] Laboratory of Neuro Imaging, University of California-Los Angeles, School of Medicine, 635 Charles Young Drive South, Suite 225, Los Angeles, CA 90095-7334, USA

Corresponding author:

Iman Aganj

200 Union St. SE, Minneapolis, MN 55455, USA

Tel: +1 (612) 202-3019

Email: iman@umn.edu

**ABSTRACT**

A global probabilistic fiber tracking approach based on the voting process provided by the *Hough transform* is introduced in this work. The proposed framework tests candidate 3D curves in the volume, assigning to each one a score computed from the diffusion images, and then selects the curves with the highest scores as the potential anatomical connections. The algorithm avoids local minima by performing an exhaustive search at the desired resolution. The technique is easily extended to *multiple* subjects, considering a single representative volume where the registered high-angular resolution diffusion images (HARDI) from all the subjects are non-linearly combined, thereby obtaining population-representative tracts. The tractography algorithm is run only once for the multiple subjects, and no tract alignment is necessary. We present experimental results on HARDI volumes, ranging from a 1.5T physical phantom to 7T and 4T human brain and 7T monkey brain datasets.

Keywords: Tractography, diffusion-weighted magnetic resonance imaging (DWI), Hough transform, orientation distribution function (ODF), population studies.

## 1. Introduction

Understanding the connectivity between different areas of the brain is essential in studying brain function and development. Diffusion-weighted magnetic resonance imaging (DWI) provides, through tractography, a unique *in-vivo* quantitative measurement of the brain's anatomical connectivity. In addition to its benefits in neurosurgical planning, DWI tractography has considerable clinical importance by noninvasively quantifying changes in the white matter connectivity at different stages of diseases or development. Moreover, it can be used to segment fiber bundles of the central nervous system, or in tract-based statistical analysis of scalars such as the fractional anisotropy (FA). Performing tractography in multiple subjects is invaluable for population studies and creating fiber bundle atlases.

DWI provides local information about the fiber orientation by measuring the tissue water diffusion, *in vivo*, assuming a high correlation between the fiber and diffusion orientations. However, there is no unique solution as to how to integrate these voxel-scale local orientations to infer global connectivity. Early fiber tractography algorithms, known as streamline methods, are based on following the principal diffusion orientation (Basser et al., 2000; Conturo et al., 1999; Jones et al., 1999; Lazar et al., 2003; Mori et al., 1999). Despite their simplicity, these methods are prone to cumulative errors caused by noise, partial volume effects, and discrete integration, and have difficulty in distinguishing fiber crossing and kissing mostly due to the fact that the entire diffusion information is not globally used and integrated. This led to the development of other successful approaches, including probabilistic techniques (Behrens et al., 2007; Björnemo et al., 2002; Descoteaux et al., 2009; Friman et al., 2006; Jones, 2008; Lazar & Alexander, 2005; Parker et al., 2003),global techniques based on front propagation (Campbell et al., 2005; Jackowski et al., 2005; Parker et al., 2002; Pichon et al., 2005; Prados et al., 2006; Tournier et al., 2003), simulation of the diffusion process or fluid flow (Batchelor et al., 2001; Hageman et al., 2009; Hagmann et al., 2003; Kang et al., 2005; O'Donnell et al., 2002; Yörük et al., 2005), DWI geodesic computations (Jbabdi et al., 2008; Lenglet et al., 2009a; Melonakos et al., 2007; Pechaud et al., 2009), graph theoretical techniques (Iturria-Medina et al., 2007; Sotiropoulos et al., 2009; Zalesky, 2008), spin glass models (Fillard et al., 2009; Mangin et al., 2002), and Gibbs tracking (Kreher et al., 2008). Generally speaking, for virtually every tractography method, a particular putative *subset* of all possible curves is implicitly considered from which the resulting tracts are chosen according to some criteria. This subset, although different depending on the particular sweeping strategy, virtually never coincides with the *universal* set of all possible curves representing the candidate tracts. The closer the subset is to the universal set of curves, the more accurate we expect the results to be. For a recent thorough discussion on different tractography techniques, see (Behrens & Jbabdi, 2009).

Prior approaches for multi-subject tractography are typically based on the post processing of tractography results from individual subjects (El Kouby et al., 2005; Jbabdi et al., 2009; Leemans et al., 2006; Maddah et al., 2006; O'Donnell & Westin, 2007; Voineskos et al., 2009; Wakana et al., 2004). These methods generally require aligning the tracts and mapping them into a common fiber coordinate system, which is challenging due to the large number of high-dimensional fiber trajectories per subject and the lack of clearly defined criteria for aligning curves and particularly tracts.

In this work, we present a global probabilistic approach inspired by the voting procedure provided by the popular *Hough transform* (Duda & Hart, 1972; Gonzalez & Woods, 2008). Our proposed tractography algorithm essentially tests candidate 3D curves in the volume, assigning a score to each of them, and then returning the curves with the highest scores as the potential anatomical connections. The score is accordingly derived from the DWI data. Being an exhaustive search, this proposed algorithm avoids entrapment in local minima within the discretization resolution of the parameter space.[1] Furthermore, the specific definition of the candidate tract score has the desired effect of attenuating the noise through the integration of the real-valued local votes derived from the diffusion data. We also introduce a simultaneous *multi-subject* tractography technique which takes as input a single representative volume – where the HARDI data from all the (registered) subjects are non-linearly integrated – and generates population-representative tracts. The multi-subject tractography algorithm is run only once, and no tract alignment is necessary. We present experimental results on HARDI volumes such as a biological phantom dataset acquired at 1.5T, a monkey brain dataset acquired at 7T, and a number of human brain datasets acquired at 4T and 7T.[2]

In Sec. 2 we present the proposed algorithm in detail. Experimental results are presented in Sec. 3, and Sec. 4 concludes with a review of the contributions. Additional implementation details are provided in the Appendix.

## 2. Methods

We first randomly generate a sufficiently high number of initial seed points inside a brain mask or a region of interest. From each initial point, we consider as many passing curves as desired, based on the expected resolution and available computational resources (Fig. 1, left). A score is computed for each

[1] Please note that many prior approaches may as well be modified to perform efficient exhaustive searches.

[2] This paper extends our previous conference versions for single and multiple subjects (Aganj et al., 2009a,b). In particular, we provide more implementation details and additional validation and comparisons.

curve, and the one (or ones) with the maximum score is then chosen as the best curve(s) representing the fiber bundle passing through that seed point (Fig. 1, middle & right).[3] This process is detailed in the following subsections.

*2.1. Curve parameterization*

We parameterize the 3D curves by the arc length $s$, with $s = 0$ corresponding to the seed point (Fig. 2). The unit tangent vector of the curve is identified at each point by standard polar coordinates $\theta(s)$ and $\phi(s)$:

$$\hat{t}(s) = \begin{pmatrix} \sin\theta(s)\cos\phi(s) \\ \sin\theta(s)\sin\phi(s) \\ \cos\theta(s) \end{pmatrix}. \quad (1)$$

In our proposed model, we consider simple polynomial approximations of these two angles with respect to the arc length:

$$\theta(s) = \sum_{k=0}^{N} a_k s^k, \quad (2)$$

$$\phi(s) = \sum_{k=0}^{N} b_k s^k, \quad (3)$$

where $N$ is the polynomial order (different orders for $\theta$ and $\phi$ can be considered if desired). The Hough-inspired process will be used to select the best possible coefficients $a_k$ and $b_k$ (and the two additional parameters introduced below), based on the available diffusion data. In addition, two extra parameters $L_-$ and $L_+$ determine the partial (Euclidean) lengths of the curve on each side of the seed point (Fig. 2), with $0 \leq L_{-,+} \leq L_{max}$ where the constant $L_{max}$ is chosen as the maximum expected curve (fiber) length. Each curve initiated from the seed point $\vec{x}_0$ is then represented using $d = 2N + 4$ unique parameters, $\{a_0, \dots, a_N, b_0, \dots, b_N, L_-, L_+\}$, and explicitly computed by integrating the tangent vector:

[3] As customary in probabilistic techniques, several candidate curves may as well be selected per seed point, each carrying a score.

$$\vec{x}(s) = \vec{x}_0 + \int_0^s \hat{t}(s')ds', \qquad s \in [-L_-, L_+]. \tag{4}$$

*2.2. Fiber score computation*

A score, intended to estimate the log-probability of the existence of a fiber, is assigned to each possible 3D curve passing through a seed point $\vec{x}_0$. In this work, the score is defined as

$$\begin{aligned} S_{\vec{x}_0}(a_0, \dots, a_N, b_0, \dots, b_N, L_-, L_+) &\coloneqq \int_{-L_-}^{L_+} \left(\log P\left(\vec{x}(s), \hat{t}(s)\right) + \lambda\right) ds \\ &= \int_{-L_-}^{L_+} \log P\left(\vec{x}(s), \hat{t}(s)\right) ds + \lambda(L_- + L_+). \end{aligned} \tag{5}$$

The expression $P(\vec{x}, \hat{t})d\Omega$ represents the probability for the point $\vec{x}$ to be located inside a fiber bundle passing in the direction $\hat{t}$ through the infinitesimal solid angle $d\Omega$.[4] The constant $\lambda$, which is used to compensate for the absence of $d\Omega$ in the integral, can also be interpreted as a prior on the length of the fiber bundles, as choosing a larger $\lambda$ favors the score of longer curves.[5]

$P(\vec{x}, \hat{t})$ can be computed using the conditional probability formula as,

$$P(\vec{x}, \hat{t}) = P(\vec{x})P(\hat{t}|\vec{x}). \tag{6}$$

The prior probability of the existence of a fiber at the point $\vec{x}$, $P(\vec{x})$, is considered to be equal to either the fractional anisotropy (FA) or generalized fractional anisotropy (GFA) inside the brain tissue, and zero outside the brain mask and inside the cerebrospinal fluid. This comes from the assumption that the more anisotropic a region is, the more likely a fiber bundle may be passing through that region. In addition, as long as no further constraints or selections are provided by the user, the initial seed points are chosen

[4] The curve score is defined by assuming that adjacent voxels are independent, making it only an approximation of the true fiber log-probability. The incorporation of spatial coherence and continuity is the subject of future research.

[5] Not including $\lambda$ may cause the zero-length curve ($L_- = L_+ = 0$) to gain the maximum score, due to the potentially negative values of the logarithm.

randomly with a spatial probability distribution proportional to $P(\vec{x})$. Other choices for $P(\vec{x})$, such as the white matter complexity introduced in (Haro et al., 2008), are also possible.

Next, assuming that a fiber is actually passing through the point $\vec{x}$, the probability for it to be in the direction $\hat{t}$, i.e. $P(\hat{t}|\vec{x})$, is derived from the orientation distribution function (ODF) at each voxel in the volume. Computed from various DWI modalities, the ODF is defined as,

$$ODF(\hat{u}) \coloneqq \int_0^\infty PDF(r\hat{u})r^2 dr, \tag{7}$$

which is the integration of the $PDF(\vec{r})$ (the spatial probability density function of the diffusion of water after a certain amount of time), in a cone of constant solid angle (CSA) in the direction of the unit vector $\hat{u}$. In Diffusion Spectrum Imaging (DSI) (Wedeen et al., 2005), $PDF(\vec{r})$ is available on a discrete Cartesian grid, and therefore the ODF is directly computed from the above formula. In the case of the Diffusion Tensor Imaging (DTI) (Basser et al., 1994), the ODF is computed by integrating the 3D normal distribution,

$$\underset{\text{in DTI}}{ODF}(\hat{u}) = \int_0^\infty \frac{1}{(2\pi)^{\frac{3}{2}}|D|^{\frac{1}{2}}} e^{-\frac{1}{2}r\hat{u}^T D^{-1} r\hat{u}} r^2 dr = \frac{1}{4\pi|D|^{\frac{1}{2}}(\hat{u}^T D^{-1}\hat{u})^{\frac{3}{2}}}, \tag{8}$$

where $D$ is proportional to the estimated diffusion tensor.

In this work, however, we use Q-ball Imaging (QBI) (Tuch, 2004), which is a popular HARDI reconstruction method proven successful in resolving multiple intravoxel fiber orientations. The original ODF expression in QBI does not include the Jacobian factor $r^2$, creating the need for post-processing such as artificial sharpening. Here we use the normalized and dimensionless ODF estimator in QBI, derived in (Aganj et al., 2010), which by considering the factor $r^2$ computes the CSA-ODF,

$$\underset{\text{in CSA-QBI}}{ODF}(\hat{u}) \approx \frac{1}{4\pi} + \frac{1}{16\pi^2}\,\text{FRT}\left\{\nabla_b^2 \ln\left(-\ln\frac{S(\hat{u})}{S_0}\right)\right\}, \tag{9}$$

with $S(\hat{u})$ and $S_0$ the diffusion signal and the baseline image respectively, and FRT and $\nabla_b^2$ the Funk-Radon transform (Funk, 1916) and the Laplace-Beltrami operator respectively. This ODF reconstruction scheme has been shown to outperform the original QBI by improving the resolution of multiple fiber orientations (Aganj et al., 2010), and producing more stable and consistent GFA (Fritzsche et al., 2010). To allow sampling in any desired direction $\hat{t}$, the ODFs were approximated in the real and symmetric

modified spherical harmonic basis, following the method proposed by Descoteaux et al. (2007) for the original QBI, and subsequently adapted in (Aganj et al., 2010) for the CSA-QBI.

Putting all this together, and using for instance the FA as $P(\vec{x})$, the score in Eq. (5) thus becomes,

$$S_{\vec{x}_0}(a_0, \dots, a_N, b_0, \dots, b_N, L_-, L_+) \coloneqq \int_{-L_-}^{L_+} \left(\log\left[ODF_{\vec{x}(s)}\left(\hat{t}(s)\right)FA\left(\vec{x}(s)\right)\right] + \lambda\right)ds, \tag{10}$$

where $ODF_{\vec{x}(s)}\left(\hat{t}(s)\right)$ stands for the ODF at the 3D position $\vec{x}(s)$ evaluated in the direction $\hat{t}(s)$, with $\vec{x}(s)$ and $\hat{t}(s)$ represented via the polynomials as specified in equations (1–4). The score integral in equations (5) and (10) has the additional nice effect of attenuating the additive noise in the data through summation.

### *2.3. Hough transform*

As discussed in Sec. 2.1, every curve starting from a particular seed point is presented as a point in a $d$-dimensional space, with $d = 2N + 4$ being the number of necessary parameters. In theory, we would like to find all possible curves which pass through the seed point while computing their scores, to eventually choose the one(s) with the highest score(s) as the potential fiber tract(s) passing through the seed point. However, we can only perform such an exhaustive search within a finite resolution, by discretizing $\mathbb{R}^d$ and assigning discrete values to the curve parameters within some predefined limits.[6] The resulting $d$-dimensional array of curve scores is often called the *Hough transform* (Duda & Hart, 1972; Gonzalez & Woods, 2008) of the data with respect to the curves passing through the chosen seed point. This can be seen as a voting process where the voxels cast real-valued votes for the curves. The overall vote is the integrand of the score integral (Eq. (5) or (10)) if a curve passes through a voxel, and zero otherwise.

The proposed method avoids entrapment in local minima by performing an exhaustive search in the (discretized) high-dimensional space of the curves. Nevertheless, the discretization resolution of the parameter space causes the algorithm to obtain an approximation of the true global optimum (which is improved by increasing the resolution as desired). To alleviate this issue, we choose the best curve in a multi-resolution approach: once the point (in the parameter space $\mathbb{R}^d$) corresponding to the curve with the highest score is found in one resolution level, the neighborhood of that point is discretized again with a

[6] This is the standard procedure in the Hough transform, where the accumulator is discretized.

higher resolution and the search is continued at the next level. We have performed our experiments using three levels of resolution.

This concludes the description of the proposed technique for a single dataset. We now show how this can be efficiently extended to multiple datasets or subjects.

### *2.4. Extension to multiple subjects*

Here we extend our Hough transform-based global approach to obtain average representative tracts from multiple subjects or datasets. We perform this by first registering the HARDI volumes, using either linear transformation or more sophisticated algorithms such as (Chiang et al., 2008), and then running the algorithm described above on a single equivalent volume composed of the voxel-wise mean ODF and mean FA across all the subjects.[7] We may use either the arithmetic or the geometric mean, however, the linearity of the curve score (Eq. (10)) with respect to the logarithms of the ODF and FA makes the use of the geometric mean more appealing (since the arithmetic mean of the logarithms of the ODF and FA values equals the logarithm of their geometric mean). Hence, we reconstruct the effective ODF and FA for each voxel by computing the geometric mean of their values across the subjects,

$$ODF_{\vec{x}}^{eq}(\hat{t}) \coloneqq \left(\prod_{i=1}^{M} ODF_{\vec{x}}^{i}(\hat{t})\right)^{\frac{1}{M}}, \tag{11}$$

$$FA^{eq}(\vec{x}) \coloneqq \left(\prod_{i=1}^{M} FA^{i}(\vec{x})\right)^{\frac{1}{M}}, \tag{12}$$

where the superscripts $i$ and $eq$ indicate respectively the $i^{th}$ subject (out of a total of $M$) and the *equivalent* subject. We eventually use the equivalent ODF and FA volumes in the single-subject tractography algorithm, thereby running it only once for all the subjects and avoiding complications due to curve (tracts) registration.

[7] This could be interpreted as multiple votes per voxel, cast by each corresponding voxel in each volume.

## 3. Experimental results and discussion

### *3.1. Results for single subjects*

We tested our method on various HARDI datasets, for each of which the FA and the CSA-ODFs were computed as explained in Sec. 2.2.

We first used the biological phantom in (Campbell et al., 2005), constructed from excised rat spinal cords and designed to have crossing tracts (90 diffusion images at b = 1300 s/mm², 1.5T). We computed the tracts from 200 seed points, using three different bias values of $\lambda$ = 2.0, 2.5, and 3.0 (see Sec. 2.2), and polynomials of order $N = 3$, resulting in a total number of $d = 10$ parameters to represent the candidate 3D curves initiated from each seed point. Figure 3 (top, left) shows the ODFs superimposed on the FA map, and the rest of the subfigures show the tractography results using different values for $\lambda$. Increasing $\lambda$ results in longer curves being selected. The color and the opacity of each tract (in all the figures) increase with the score, from transparent blue to opaque red.

We performed additional experiments on a human brain HARDI dataset acquired at 7T. A single refocused 2D single shot spin echo EPI sequence was used. Image parameters were: FOV: 192×192 $mm^2$ (matrix: 196×96) to yield a spatial resolution of 2×2×2 $mm^3$, TR/TE 4800/57 msec., acceleration factor (GRAPPA) of 2 and 6/8 partial Fourier were used along the phase encode direction. Diffusion-weighted images were acquired at b = 3000 s/$mm^2$ with 256 directions, along with 31 baseline images. EPI echo spacing was 0.57 msec. with a bandwidth of 2895 Hz/Pixel. Tracts were computed from 1500 seed points in two experiments, using polynomials of orders $N = 2$ and $N = 3$ (Fig. 4). High scoring curves are concentrated in major fiber bundles such as corona radiata, corpus callosum, cingulum, superior longitudinal fasciculus, and arcuate fasciculus. Higher polynomial order brings more flexibility to the curves, resulting in them being spread out more continuously in the white matter regions (e.g. in corona radiata). A 3D stereoscopic rendering of the results is shown in Fig. 5.

Next, we used the monkey brain HARDI dataset introduced in (Lenglet et al., 2009b) to test the performance of our method on specific fiber bundles. An anesthetized Macaca mulatta monkey was scanned using a 7T MR scanner (Siemens) equipped with a head gradient coil (80mT/m G-maximum, 200mT/m/ms) with a diffusion weighted spin-echo EPI sequence. Diffusion images were acquired at b = 3000 s/mm² (twice during the same session, and then averaged) over 100 directions uniformly distributed on the sphere. We used TR/TE of 4600/65 ms, and a voxel size of 1×1×1 mm³. We computed the tracts from 1350 seed points uniformly distributed in a mask containing the intersection of the forceps minor and the inferior longitudinal fasciculus, using the polynomials of order $N = 3$. Results are depicted in Fig. 6. A fiber density map was created by counting, at each voxel, the number of intersecting curves

while taking into account their respective score. A three-dimensional isosurface was then generated by thresholding this map to keep the most relevant connections. It is as well presented in Fig. 6, overlaid on a structural MRI. Major tracts including the splenium fibers, posterior corona radiata, tapetum, as well as the inferior fronto-occipital and longitudinal fasciculi – including the optic radiations – are clearly identified. Moreover, fibers of the optic tract are recovered until they reach the optic chiasm.

### *3.2. Results for multiple subjects*

We used our multi-subject tractography algorithm to compute mean tracts from five HARDI datasets, introduced in (de Zubicaray et al., 2008), each acquired from a different healthy young adult. Images were acquired using a 4T Bruker Medspec MRI scanner. Diffusion-weighted images were acquired using single-shot echo planar imaging with a twice-refocused spin echo sequence to reduce eddy-current induced distortions. Imaging parameters were: 23 cm FOV, TR/TE 6090/91.7 ms, with a 128×100 acquisition matrix. Each 3D volume consisted of 55 2-mm thick axial slices with a 1.8×1.8 mm² in-plane resolution. 105 images were acquired: 11 with no diffusion sensitization (i.e., T2-weighted $b_0$ images) and 94 diffusion-weighted images (b = 1159 s/mm²) with gradient directions evenly distributed on the hemisphere. Scan time was approximately 14 minutes. Images were corrected for motion and eddy current distortions. Each subject's average $b_0$ image was aligned to a group-specific minimal deformation template (MDT) using a nine-parameter affine transformation. This transformation was then applied to each individual DWI and gradient directions were corrected accordingly for ODF calculations.

We combined the individual datasets into two equivalent volumes, using the geometric and the arithmetic means (see Sec. 2.4). We tested the tractography algorithm on both equivalent volumes, and also for comparison, on two of the five individual datasets. In each experiment, polynomials of order $N = 3$ were used to represent 3D tracts initiated from 1500 seed points. Figure 7 (two top rows) show the mean tracts from the five subjects using respectively the geometric and arithmetic means. The two bottom subfigures show tracts from individual subjects. As Fig. 7 demonstrates, combining the volumes improves the results by decreasing the number of false positives produced by noise. In addition, the fibers are less scattered and better concentrated in major fiber bundles. Note particularly how corticospinal tracts are enhanced.

## 4. Conclusion

We have introduced a global approach for single- and multi-subject probabilistic tractography, based on the voting process provided by the Hough transform. We presented experimental results on a physical phantom and brain HARDI datasets, and showed that using this approach, data from multiple subjects can be non-linearly combined and exploited to obtain population statistics and more accurate tractography results. The incorporation of spatial coherence and continuity in curve score computation is the subject of future research.


## Acknowledgments

This work was partly supported by NIH (P41 RR008079, P30 NS057091, R01 HD050735, R01 EB007813, R01 MH060662, R01 EB008432, R01 EB008645, CON000000004051–3014, CON000000015793–3014, NLM T15 LM07356), NSF, ONR, NGA, ARO, and DARPA. Computing resources were provided by the University of Minnesota Supercomputing Institute, and the Laboratory of Neuro Imaging (UCLA). We would like to thank Jennifer Campbell of McGill University, Katie L. McMahon and Greig I. de Zubicaray of the Centre for Magnetic Resonance, University of Queensland, and Margaret J. Wright of Queensland Institute of Medical Research for providing us with HARDI data.


## Appendix

In this appendix, we provide additional details on the implementation of the proposed tractography technique.

The *Hough transform* is often used in global optimization problems to avoid local optimum solutions. This approach is however characterized by its high computational complexity, given that in a straightforward implementation, all possible solutions must be tested in order to reconstruct the table of scores. This issue could yet be alleviated by parallelizing the exhaustive searches at the seed points, as they can be computed independently of one another. Also note that the (potentially) high-dimensional table of scores need *not* be stored in computer memory, since the maximum score can be computed on the fly, thus circumventing any memory exhaustion.

A question which may arise while implementing the proposed algorithm, is whether all the polynomial coefficients should have the same discretization resolution, and if not, how to determine it.

From Eq. (2) it can be seen that the small change $\Delta a_k$ in the $k^{th}$ coefficient (due to its discretization resolution) results in the following change in $\theta$ at the arc length $s$:

$$\Delta\theta(s) = \Delta a_k s^k \tag{A.1}$$

Ideally, we would like a uniform resolution for $\theta$, which would mean that $\Delta\theta(s)$ needs to be independent of $s$ and $k$. Although this dependency cannot be eliminated, it can be minimized by choosing a specific value for $\Delta a_k$. Assuming the desired constant value $\delta$ for $\Delta\theta(s)$, we minimize the following squared error integral to obtain the optimum value $\Delta a_k^*$:

$$\begin{aligned} \Delta a_k^* &= \underset{\Delta a_k}{\operatorname{argmin}} \int_{-L_{max}}^{L_{max}} (|\Delta\theta(s)| - \delta)^2 ds \\ &= \underset{\Delta a_k}{\operatorname{argmin}} \int_{-L_{max}}^{L_{max}} \left(\left|\Delta a_k s^k\right| - \delta\right)^2 ds \\ &= \frac{\delta}{L_{max}^k}\left(2 - \frac{1}{k+1}\right). \end{aligned} \tag{A.2}$$

By choosing such resolutions for the polynomial coefficients $a_k$, and similarly for $b_k$, the curve space is discretized more uniformly, hence increasing the accuracy of the search for the high scoring curves.

**References**


Aganj, I., Lenglet, C., Keriven, R., Sapiro, G., Harel, N. & Thompson, P.M., 2009a. A Hough transform global approach to diffusion MRI tractography. In *Proc. of 17th Annual Meeting of ISMRM*, Honolulu.

Aganj, I., Lenglet, C., Sapiro, G., Chiang, M.C. & Thompson, P.M., 2009b. Multi-subject diffusion MRI tractography via a Hough transform global approach. In *Proc. of 15th Annual Meeting of OHBM*, San Francisco.

Aganj, I., Lenglet, C., Sapiro, G., Yacoub, E., Ugurbil, K. & Harel, N., 2010. Reconstruction of the orientation distribution function in single and multiple shell q-ball imaging within constant solid angle. *Magnetic Resonance in Medicine*, in press.

Basser, P.J., Mattiello, J. & LeBihan, D., 1994. Estimation of the effective self-diffusion tensor from the NMR spin echo. *J Magn Reson B.*, 103(3), p.247–254.

Basser, P.J., Pajevic, S., Pierpaoli, C., Duda, J. & Aldroubi, A., 2000. In vivo fiber tractography using DT-MRI data. *Magnetic Resonance in Medicine*, 44(4), p.625–632.

Batchelor, P.G., Hill, D.L.G., Atkinson, D. & Calamante, F., 2001. Study of connectivity in the brain using the full diffusion tensor from MRI. In *Proc. of 17th IPMI*, Davis.

Behrens, T.E.J. & Jbabdi, S., 2009. MR diffusion tractography. In *Diffusion MRI: From Quantitative Measurement to In-vivo Neuroanatomy*, 1st ed, Academic Press.

Behrens, T.E.J., Johansen Berg, H., Jbabdi, S., Rushworth, M.F.S. & Woolrich, M.W., 2007. Probabilistic diffusion tractography with multiple fibre orientations: What can we gain? *NeuroImage*, 34(1), p.144–155.

Björnemo, M., Brun, A., Kikinis, R. & Westin, C.F., 2002. Regularized stochastic white matter tractography using diffusion tensor MRI. In *Proc. of 5th MICCAI*, Tokyo.

Campbell, J.S.W., Siddiqi, K., Rymar, V.V., Sadikot, A.F. & Pike, G.B., 2005. Flow-based fiber tracking with diffusion tensor and q-ball data: Validation and comparison to principal diffusion direction techniques. *NeuroImage*, 27(4), p.725–736.

Chiang, M.C. et al., 2008. Brain fiber architecture, genetics, and intelligence: A high angular resolution diffusion imaging (HARDI) study. In *Proc. of 11th MICCAI*, New York.

Conturo, T.E. et al., 1999. Tracking neuronal fiber pathways in the living human brain. *Proc. of National Academy of Sciences*, 96(18), p.10422–10427.

de Zubicaray, G.I. et al., 2008. Meeting the Challenges of Neuroimaging Genetics. *Brain Imaging and Behavior*, 2(4), p.258–263.

Descoteaux, M., Angelino, E., Fitzgibbons, S. & Deriche, R., 2007. Regularized, fast, and robust analytical q-ball imaging. *Magnetic Resonance in Medicine*, 58(2), p.497–510.

Descoteaux, M., Deriche, R., Knösche, T.R. & Anwander, A., 2009. Deterministic and probabilistic tractography based on complex fibre orientation distributions. *IEEE Transactions on Medical Imaging*, 28(2), p.269–286.

Duda, R.O. & Hart, P.E., 1972. Use of the Hough transformation to detect lines and curves in pictures. *Commun. ACM*, 15(1).

El Kouby, V. et al., 2005. MR diffusion-based inference of a fiber bundle model from a population of subjects. In *Proc. of 8th MICCAI*, Palm Springs.

Fillard, P., Poupon, C. & Mangin, J.F., 2009. A novel global tractography algorithm based on an adaptive spin glass model. In *Proc. of 12th MICCAI*. London.

Friman, O., Farnebäck, G. & Westin, C.F., 2006. A Bayesian approach for stochastic white matter tractography. *IEEE Transactions on Medical Imaging*, 25(8), p.965–978.

Fritzsche, K.H., Laun, F.B., Meinzer, H.P. & Stieltjes, B., 2010. Opportunities and pitfalls in the quantification of fiber integrity: What can we gain from Q-ball imaging? *NeuroImage*, 51(1), p.242–251.

Funk, P., 1916. Über eine geometrische Anwendung der Abelschen Integralgleichung. *Mathematische Annalen*, 77, p.129–135.

Gonzalez, R.C. & Woods, R.E., 2008. *Digital Image Processing*, 3rd ed, Prentice Hall.

Hageman, N.S., Toga, A.W., Narr, K.L. & Shattuck, D.W., 2009. A diffusion tensor imaging tractography algorithm based on Navier–Stokes fluid mechanics. *IEEE Transactions on Medical Imaging*, 28(3), pp.348-60.

Hagmann, P. et al., 2003. DTI mapping of human brain connectivity: statistical fibre tracking and virtual dissection. *NeuroImage*, 19(3), p.545–554.

Haro, G., Lenglet, C., Sapiro, G. & Thompson, P.M., 2008. On the Non-Uniform Complexity of Brain Connectivity. In *Proc. 5th IEEE ISBI*, Paris.

Iturria-Medina, Y. et al., 2007. Characterizing brain anatomical connections using diffusion weighted MRI and graph theory. *NeuroImage*, 36(3), p.645–660.

Jackowski, M., Kao, C., Qiu, M., Constable, R. & Staib, L., 2005. White matter tractography by anisotropic wavefront evolution and diffusion tensor imaging. *Medical Image Analysis*, 9(5), p.427–440.

Jbabdi, S., Bellec, P., Toro, R., Daunizeau, J., Pelegrini-Issac, M. & Benali, H., 2008. Accurate anisotropic fast marching for diffusion-based geodesic tractography. *International Journal of Biomedical Imaging*, 2008.

Jbabdi, S., Woolrich, M.W. & Behrens, T.E.J., 2009. Multiple-subjects connectivity-based parcellation using hierarchical Dirichlet process mixture models. *NeuroImage*, 44(2), p.373–384.

Jones, D.K., 2008. Tractography gone wild: Probabilistic fibre tracking using the wild bootstrap with diffusion tensor MRI. *IEEE Transactions on Medical Imaging*, 27(9), p.1268–1274.

Jones, D.K., Simmons, A., Williams, S.C.R. & Horsfield, M.A., 1999. Non-invasive assessment of axonal fiber connectivity in the human brain via diffusion tensor MRI. *Magnetic Resonance in Medicine*, 42(1), p.37–41.

Kang, N., Zhang, J., Carlson, E.S. & Gembris, D., 2005. White matter fiber tractography via anisotropic diffusion simulation in the human brain. *IEEE Transactions on Medical Imaging*, 24(9), p.1127–1137.

Kreher, B.W., Mader, I. & Kiselev, V.G., 2008. Gibbs tracking: A novel approach for the reconstruction of neuronal pathways. *Magnetic Resonance in Medicine*, 60(4), p.953–963.

Lazar, M. & Alexander, A.L., 2005. Bootstrap white matter tractography (BOOT-TRAC). *NeuroImage*, 24(2), p.524–532.

Lazar, M. et al., 2003. White matter tractography using diffusion tensor deflection. *Human Brain Mapping*, 18(4), p.306 –321.

Leemans, A., Sijbers, J., De Backer, S., Vandervliet, E. & Parizel, P., 2006. Multiscale white matter fiber tract coregistration: a new feature-based approach to align diffusion tensor data. *Magnetic Resonance in Medicine*, 55(6), p.1414–1423.

Lenglet, C., Prados, E., Pons, J.P., Deriche, R. & Faugeras, O., 2009a. Brain connectivity mapping using riemannian geometry, control theory, and PDEs. *SIAM Journal on Imaging Sciences*, 2(2), p.285–322.

Lenglet, C. et al., 2009b. High resolution diffusion MRI on in-vivo monkey brains at 7T. In *Proc. 14th Annual Meeting of OHBM*. San Francisco.

Maddah, M., Grimson, W.E.L. & Warfield, S.K., 2006. Statistical modeling and EM clustering of white matter fiber tracts. In *Proc. of 3rd IEEE ISBI*.

Mangin, J.F. et al., 2002. A framework based on spin glass models for the inference of anatomical connectivity from diffusion-weighted MR data - a technical review. *NMR in Biomedicine*, 15(7–8), p.481–492.

Melonakos, J., Mohan, V., Niethammer, M., Smith, K., Kubicki, M. & Tannenbaum, A., 2007. Finsler tractography for white matter connectivity analysis of the cingulum bundle. In *Proc. of 10th MICCAI*, Brisbane.

Mori, S., Crain, B.J., Chacko, V.P. & Van Zijl, P.C.M., 1999. Three dimensional tracking of axonal projections in the brain by magnetic resonance imaging. *Annals of Neurology*, 45(2), p.265–269.

O'Donnell, L., Haker, S. & Westin, C.F., 2002. New approaches to estimation of white matter connectivity in diffusion tensor MRI: Elliptic PDEs and geodesics in a tensor-warped space. In *Proc. of 5th MICCAI*, Tokyo.

O'Donnell, L.J. & Westin, C.F., 2007. Automatic tractography segmentation using a high-dimensional white matter atlas. *IEEE Transactions on Medical Imaging*, 26(11), p.1562–1575.

Parker, G.J.M., Haroon, H.A. & Wheeler-Kingshott, C.A.M., 2003. A framework for a streamline-based probabilistic index of connectivity (PICo) using a structural interpretation of MRI diffusion measurements. *Journal of Magnetic Resonance Imaging*, 18(2), p.242–254.

Parker, G.J.M., Wheeler-Kingshott, C.A.M. & Barker, G.J., 2002. Estimating distributed anatomical connectivity using fast marching methods and diffusion tensor imaging. *IEEE Transactions on Medical Imaging*, 21(5), p.505–512.

Pechaud, M., Descoteaux, M. & Keriven, R., 2009. Brain connectivity using geodesics in HARDI. In *Proc. of 12th MICCAI,* London.

Pichon, E., Westin, C.F. & Tannenbaum, A.R., 2005. A Hamilton-Jacobi-Bellman approach to high angular resolution diffusion tractography. In *Proc. of 8th MICCAI,* Palm Springs.

Prados, E. et al., 2006. Control theory and fast marching methods for brain connectivity mapping. In *Proc. IEEE Conf. CVPR,* New York.

Sotiropoulos, S.N., Bai, L., Morgan, P.S., Constantinescu, C.S. & Tench, C.R., 2010. Brain tractography using q-ball imaging and graph theory: Improved connectivities through fibre crossings via a model-based approach. *NeuroImage*, 49(3).

Tournier, J.D., Calamante, F., Gadian, D.G. & Connelly, A., 2003. Diffusion-weighted magnetic resonance imaging fibre tracking using a front evolution algorithm. *NeuroImage*, 20(1), p.276–288.

Tuch, D.S., 2004. Q-ball imaging. *Magnetic Resonance in Medicine*, 52(6), p.1358–1372.

Voineskos, A.N. et al., 2009. Quantitative examination of a novel clustering method using magnetic resonance diffusion tensor tractography. *NeuroImage*, 45(2), p.370–376.

Wakana, S., Jiang, H., Nagae-Poetscher, L.M., van Zijl, P.C.M. & Mori, S., 2004. Fiber tract–based atlas of human white matter anatomy. *Radiology*, 230, p.77–87.

Wedeen, V.J., Hagmann, P., Tseng, W.I., Reese, T.G. & Weisskoff, R.M., 2005. Mapping complex tissue architecture with diffusion spectrum magnetic resonance imaging. *Magnetic Resonance in Medicine*, 54(6), p.1377–1386.

Yörük, E., Acar, B. & Bammer, R., 2005. A physical model for DT-MRI based connectivity map computation. In *Proc. of 8th MICCAI,* Palm Springs.

Zalesky, A., 2008. DT-MRI fiber tracking: a shortest paths approach. *IEEE Transactions on Medical Imaging*, 27(10), p.1458–1471.

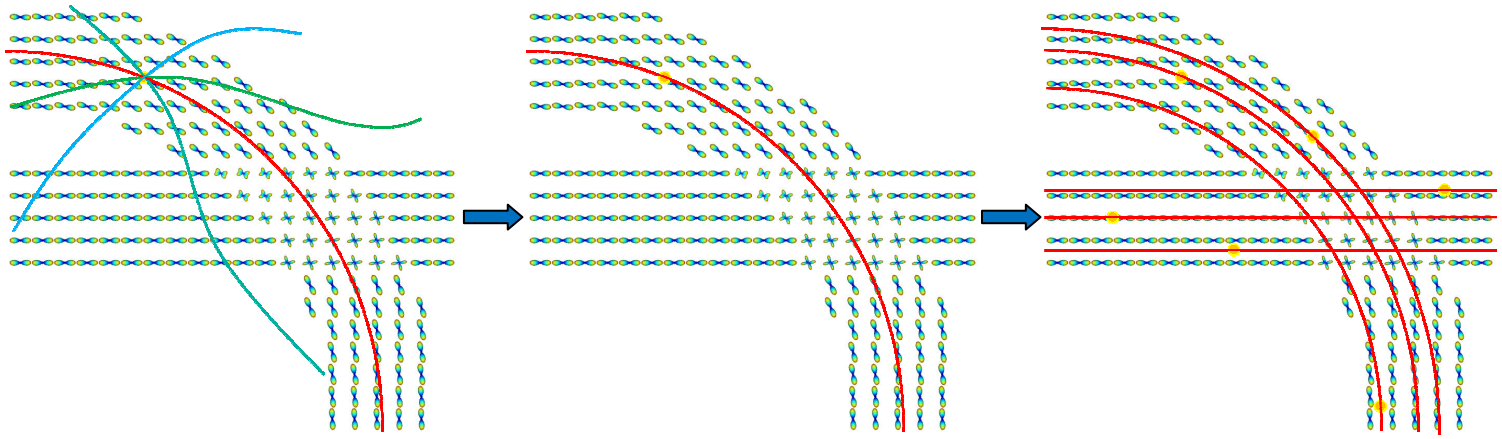

**Fig 1.** (Left) Different possible curves passing through a seed point are tested and their scores are computed. (Middle) The curve with the highest score is selected. (Right) The process is repeated for all the remaining seed points.

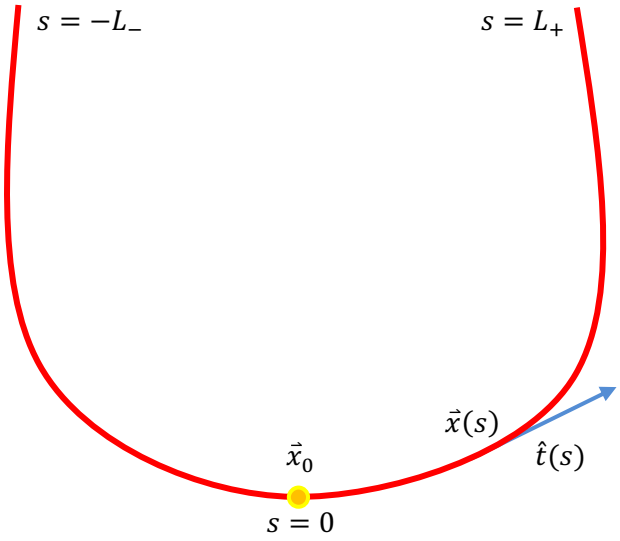


**Fig 2.** Curves starting from the seed point $\vec{x}_0$ are parameterized by the arc length, $s \in [-L_-, L_+]$. The unit tangent vector, $\hat{t}(s)$, is approximated with polynomials.

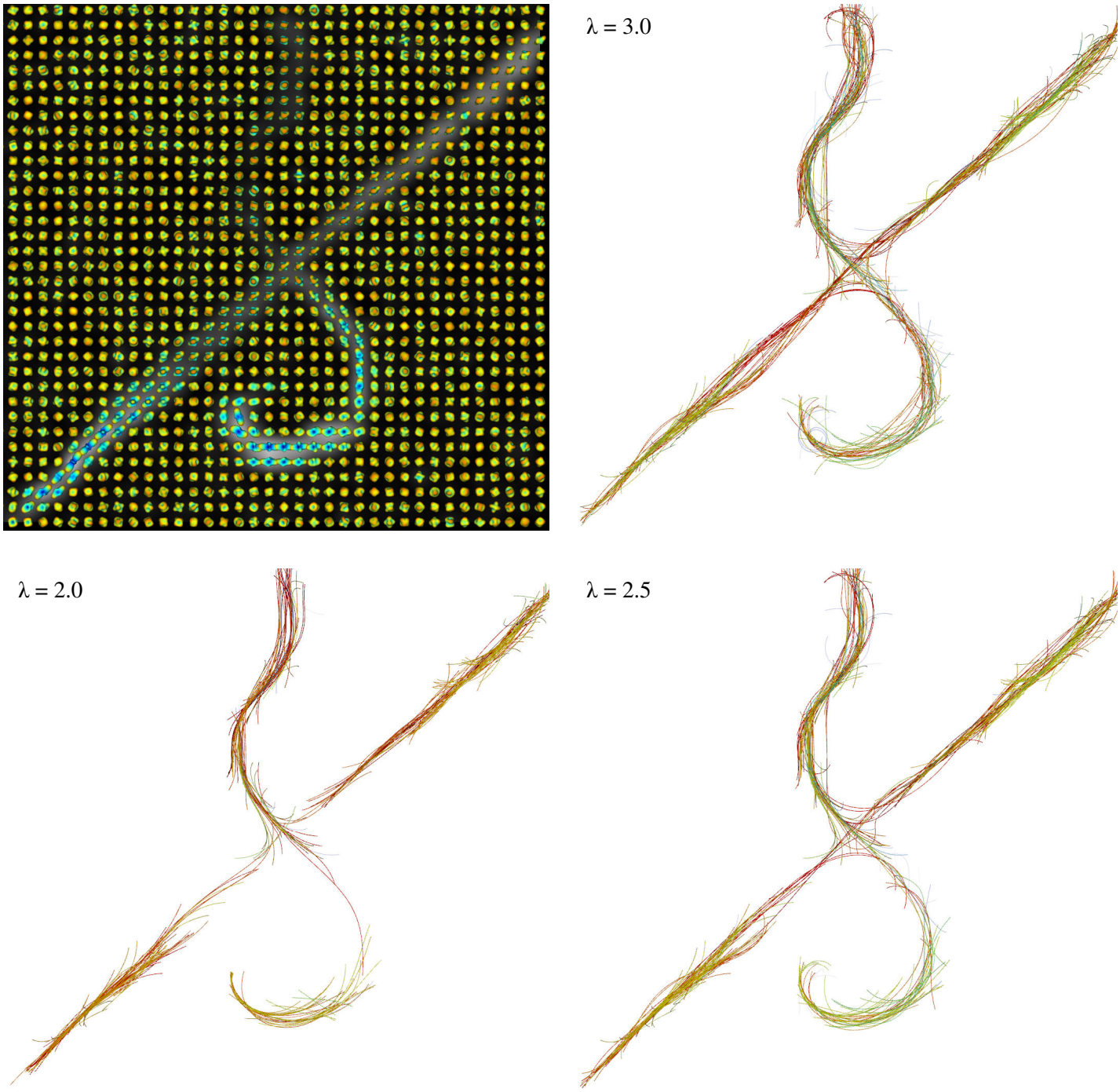


**Fig 3.** Reconstructed ODFs (top left) and the tractography results (rest of the subfigures) on the excised rat spinal cords, using various values for the bias parameter λ.

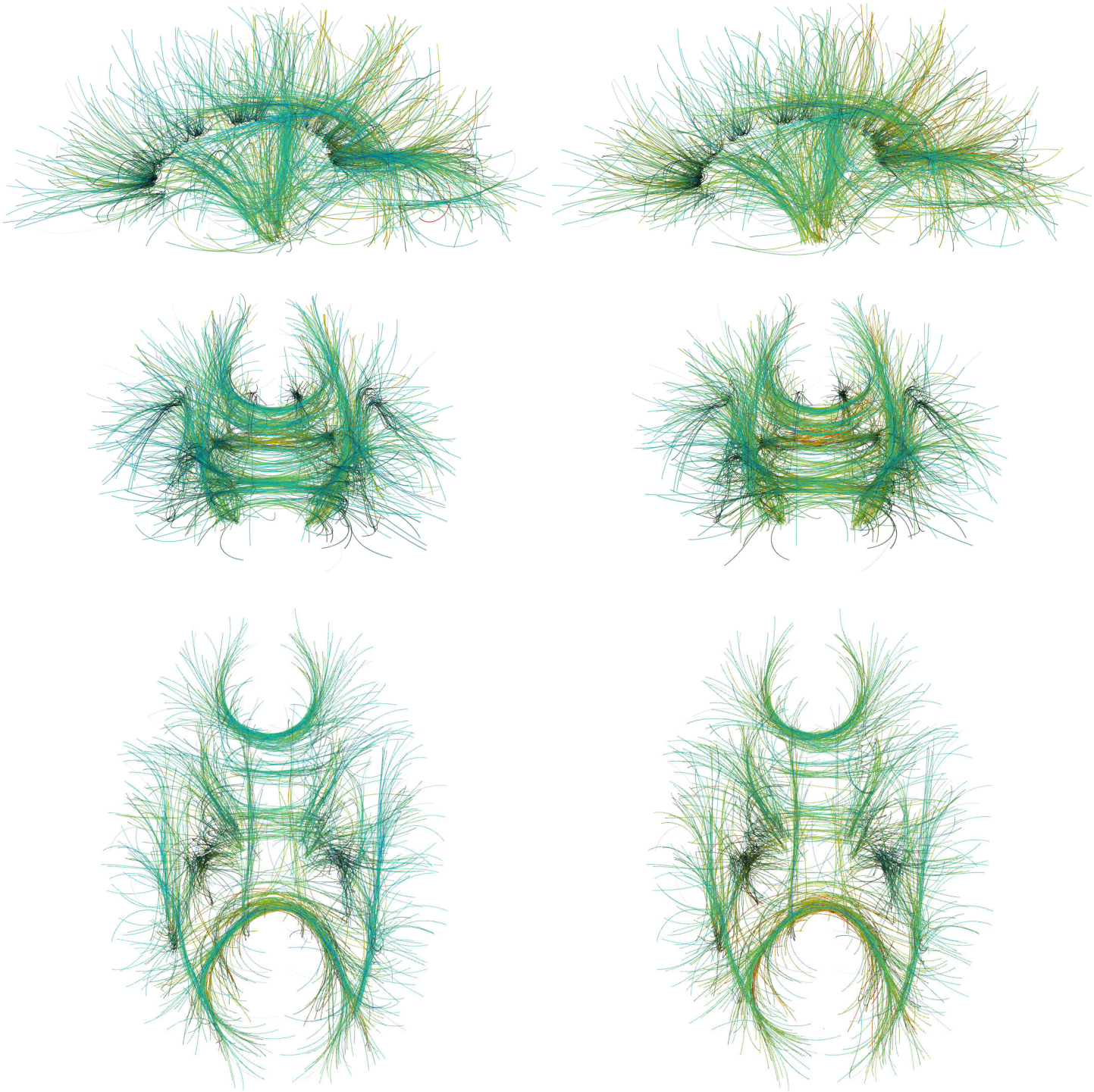

**Fig 4.** Tractography results on a human brain HARDI dataset using polynomial orders of (left) $N = 3$ and (right) $N = 2$, shown in (top) sagittal, (middle) coronal, and (bottom) axial views.

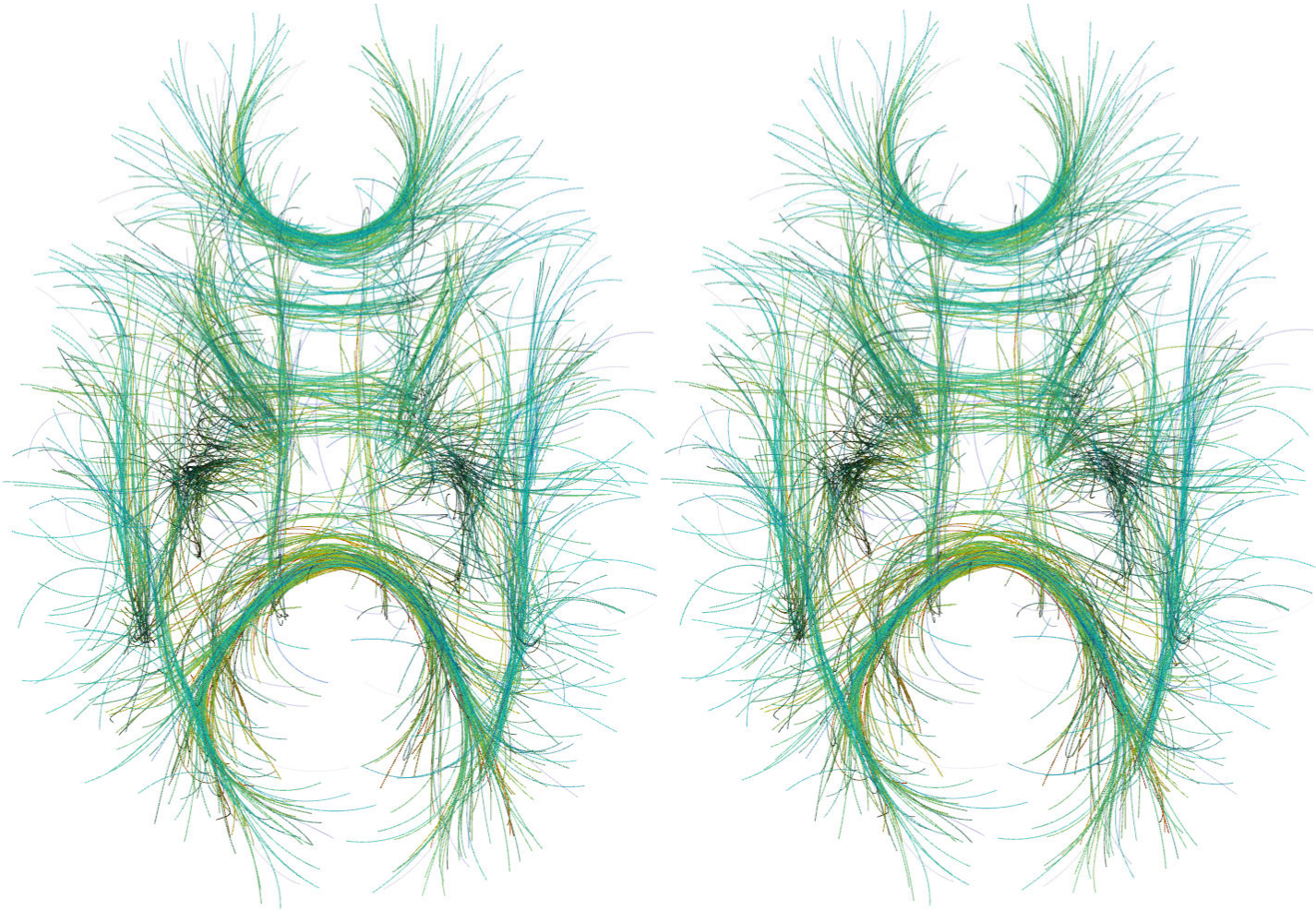

**Fig 5.** Stereoscopic rendering of Fig. 4 (bottom, left). To see this image in 3D, please cross your eyes and move the image closer or further away from you until you see what appears to be a third, 3D image in the middle.

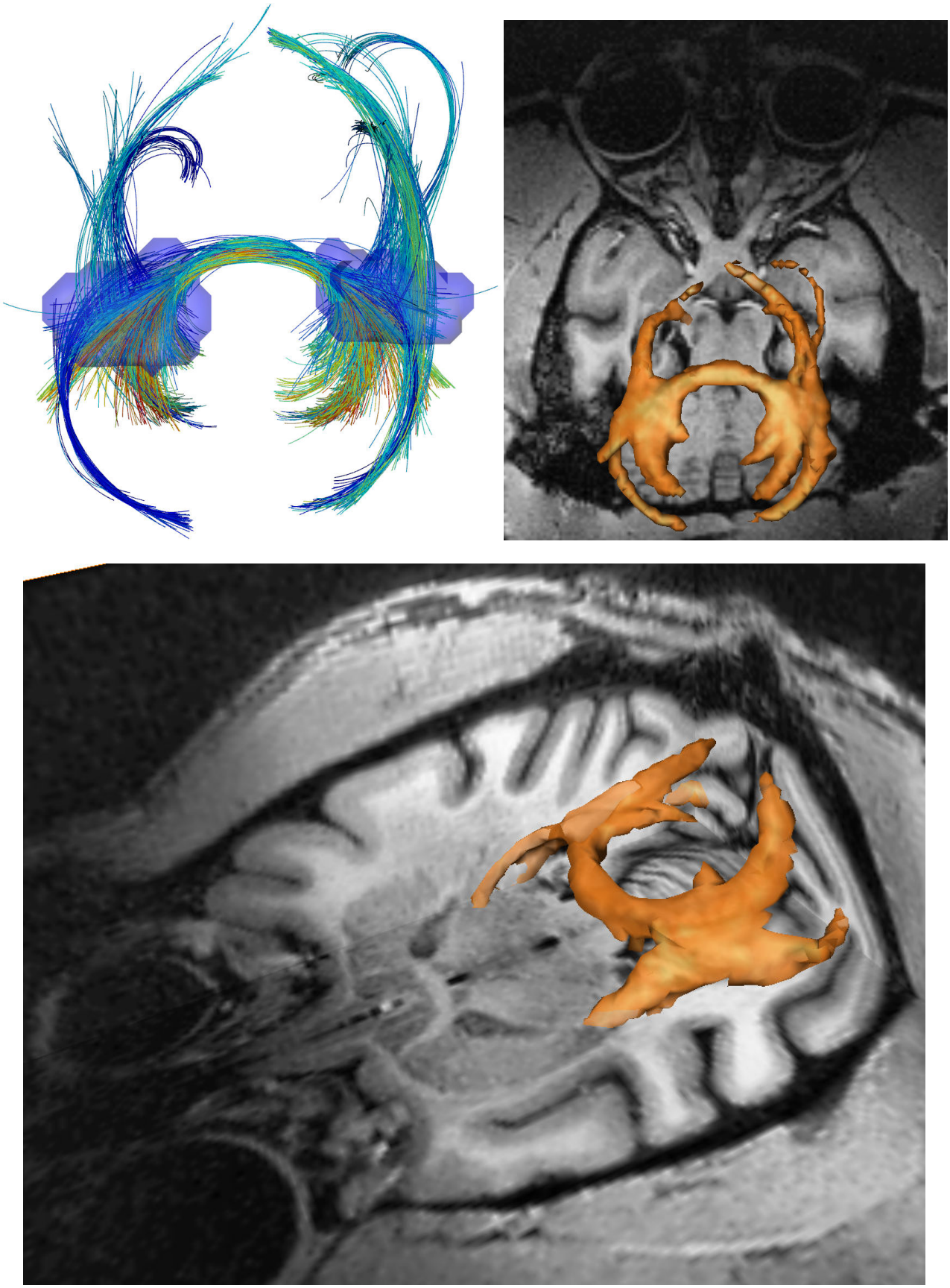

**Fig 6.** Tractography results on a monkey brain HARDI dataset shown in axial (top) and tilted (bottom) views. Seed points were randomly generated inside the transparent blue regions (top, left). A mask of the tracts is shown superimposed on the T1 anatomy image (top right & bottom).

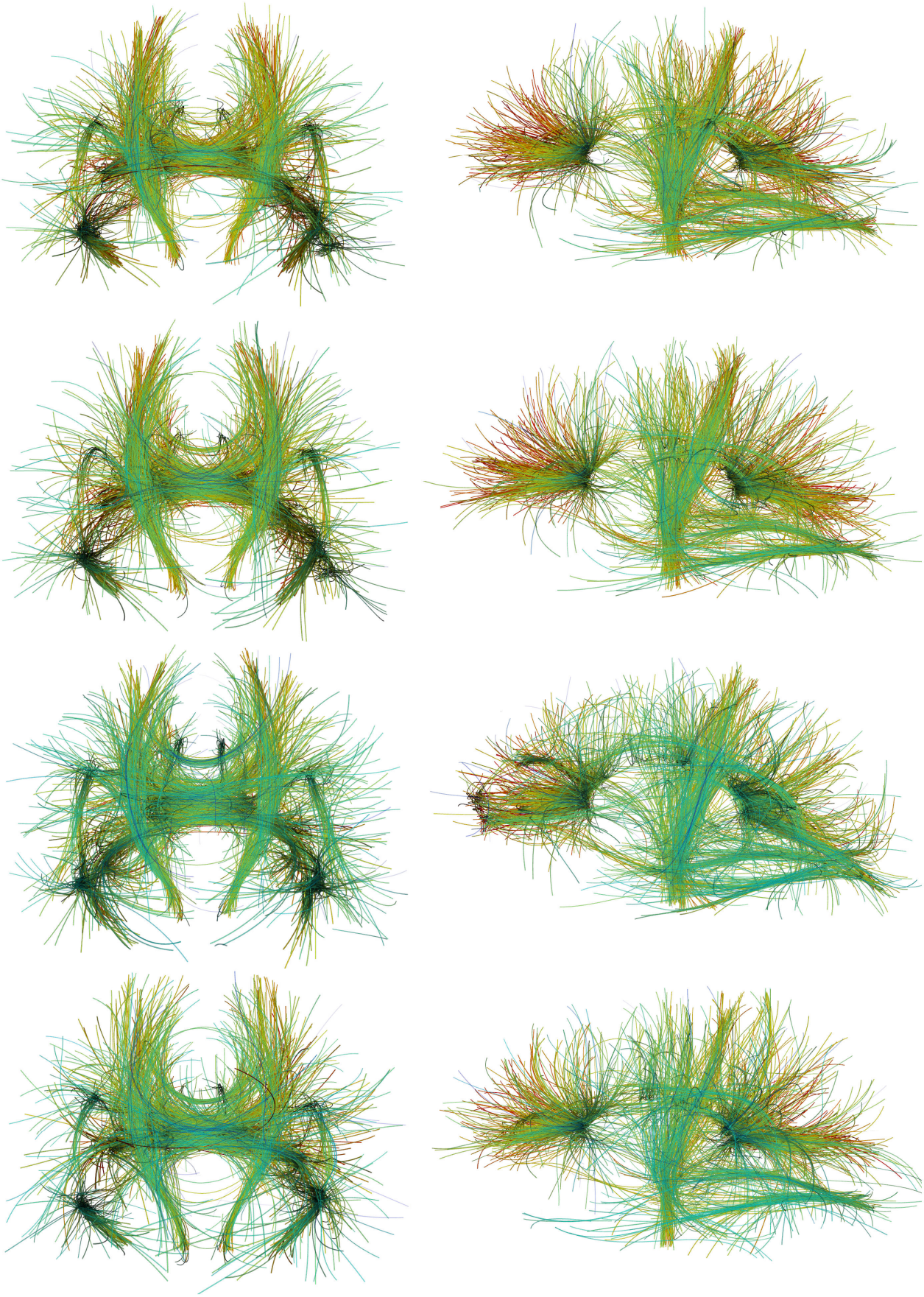

**Fig 7.** Tractography results from five human brain HARDI datasets combined using geometric (top row) and arithmetic (row two) means, and from individual subjects (two bottom rows), shown in coronal (left) and sagittal (right) views.